Computers and Geosciences 123 (2019) 137–148

Contents lists available at ScienceDirect

Computers and Geosciences

journal homepage: www.elsevier.com/locate/cageo

Integrated Object-Based Image Analysis for semi-automated geological lineament detection in southwest England

Christopher M. Yeomans[a,b,*], Maarit Middleton[c], Robin K. Shail[a], Stephen Grebby[d], Paul A.J. Lusty[b]

[a] Camborne School of Mines, College of Engineering, Maths and Physical Sciences, University of Exeter, Penryn Campus, Penryn, Cornwall, TR10 9FE, UK
[b] British Geological Survey, Environmental Science Centre, Keyworth, Nottinghamshire, NG12 5GG, UK
[c] Geological Survey of Finland, P.O. Box 77, FI-96101, Rovaniemi, Finland
[d] University of Nottingham, Nottingham Geospatial Institute, Innovation Park, Nottingham, NG7 2TU, UK

ARTICLE INFO

Keywords:
Object-based Image Analysis
Airborne geophysics
Lineament detection
Semi-automated
Southwest England

ABSTRACT

Regional lineament detection for mapping of geological structure can provide crucial information for mineral exploration. Manual methods of lineament detection are time consuming, subjective and unreliable. The use of semi-automated methods reduces the subjectivity through applying a standardised method of searching. Object-Based Image Analysis (OBIA) has become a mainstream technique for landcover classification, however, the use of OBIA methods for lineament detection is still relatively under-utilised. The Southwest England region is covered by high-resolution airborne geophysics and LiDAR data that provide an excellent opportunity to demonstrate the power of OBIA methods for lineament detection. Herein, two complementary but stand-alone OBIA methods for lineament detection are presented which both enable semi-automatic regional lineament mapping. Furthermore, these methods have been developed to integrate multiple datasets to create a composite lineament network. The top-down method uses threshold segmentation and sub-levels to create objects, whereas the bottom-up method segments the whole image before merging objects and refining these through a border assessment. Overall lineament lengths are longest when using the top-down method which also provides detailed metadata on the source dataset of the lineament. The bottom-up method is more objective and computationally efficient and only requires user knowledge to classify lineaments into *major* and *minor* groups. Both OBIA methods create a similar network of lineaments indicating that semi-automatic techniques are robust and consistent. The integration of multiple datasets from different types of spatial data to create a comprehensive, composite lineament network is an important development and demonstrates the suitability of OBIA methods for enhancing lineament detection.

1. Introduction

Mapping of geological structures can be both time-consuming and challenging in the field, particularly in areas of poor outcrop exposure. Structures such as strike-extensive faults can be particularly difficult to map by a geologist in the field due to partial exposure and subtle topographic variations. Lineament detection can aid the mapping of geological structure. A lineament is a mappable rectilinear or curvilinear linear feature of a surface, distinct from adjacent patterns, and which may represent a subsurface phenomenon (O'Leary et al., 1976). Remotely sensed data, including satellite imagery and airborne geophysical data, are commonly used for regional lineament mapping. These lineaments can be used to infer the structural geology of the region and have implications for mineral exploration (Moore and Camm, 1982; James and Moore, 1985; Ni et al., 2016), petroleum exploration (Peña and Abdelsalam, 2006), groundwater studies (Kresic, 1995; Mallast et al., 2011) and natural hazard assessment (Rutzinger et al., 2007).

Classical lineament extraction techniques include manually digitising linear features. At the regional scale, optical imagery is commonly used; however, this is time consuming and subjective and therefore lacks reproducibility (Masoud and Koike, 2006; Scheiber et al., 2015). Grebby et al. (2012) demonstrated that airborne Light Detection and Ranging (LiDAR) data can have advantages over optical

* Corresponding author. Camborne School of Mines, College of Engineering, Maths and Physical Sciences (CEMPS), University of Exeter, Penryn Campus, Penryn, Cornwall, TR10 9FE, UK.
E-mail address: c.yeomans@exeter.ac.uk (C.M. Yeomans).

https://doi.org/10.1016/j.cageo.2018.11.005
Received 21 March 2018; Received in revised form 9 September 2018; Accepted 9 November 2018
Available online 15 November 2018

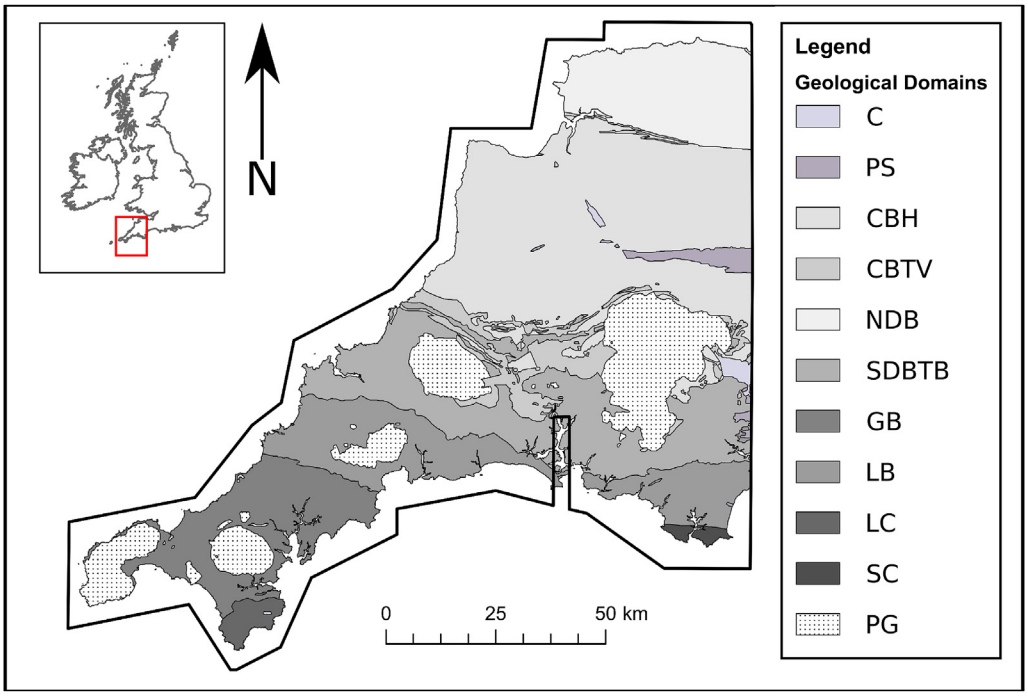

Fig. 1. Regional geology of SW England depicting the Upper Palaeozoic sedimentary basins and Permian Granites (*N.B. the Upper Devonian South Devon and Tavy basins are merged for simplicity*). The black box delimits the Tellus South West airborne geophysical data and the rectangular enclosure represents the inset over the Tamar Estuary at Her Majesty's Naval Base Devonport. C = Cenozoic; PS = Permian Sandstones; CBH = Culm Basin (Holsworthy Group); CBTV = Culm Basin (Teign Valley Group); NDB = North Devon Basin; GB = Gramscatho Basin; SDBTB = South Devon Basin and Tavy Basin; LB = Looe Basin; LC = Lizard Complex; SC = Start Complex; PG = Permian Granites. This figure includes OS data © Crown Copyright and database right (2018).

data where obstructions caused by vegetation cover can be removed to produce a Digital Terrain Model (DTM). Whilst somewhat subjective, human bias when manually digitising can be mitigated by careful data assessment (Scheiber et al., 2015), although this does not make it a less time-consuming approach.

The automation of geological lineament mapping from remotely sensed data has been a key research topic in structural geology for some decades. Automation overcomes issues of time and subjectivity that affects the manual approach. Whilst fully automatic methods are beyond the scope of current computer algorithms, semi-automated techniques are improving rapidly. Early criticisms of semi-automatic methods included the misidentification of roads and field boundaries as lineaments as well as the adverse effect of vegetation cover in some environments. These can now be circumvented with more sophisticated processing and the use of non-optical datasets such as airborne geophysics, especially magnetic data (Middleton et al., 2015), electromagnetic data (Paananen, 2013), radiometric data (Debeglia et al., 2006) and gravity data (Lahti et al., 2014).

Semi-automated mapping often makes use of an image enhancement step which can include a transform or filter. Transforms convert measurable parameters to different measurable parameters, whereas filters selectively remove undesirable data at particular frequencies (Milligan and Gunn, 1997). Enhancement filters include convolution, directional, Laplacian and Sobel filters and Principal Component Analysis (Sukumar et al., 2014). Transforms used for lineament detection can search for edges (sharp gradients) in an image (e.g. Blakely and Simpson, 1986) or the presence of elongated minima or maxima in the data (e.g. Airo and Wennerström, 2010). Transforms are more common when using potential field data such as airborne magnetic and gravity data. These often use horizontal or vertical derivatives to enhance geological edges. An effective option is the Tilt Derivative (TDR), which acts as a gain control, normalizes and enhances the continuity of structures (Verduzco et al., 2004) to help detect edges, minima or maxima (Fairhead et al., 2004; Airo and Wennerström, 2010; White and Beamish, 2011; Middleton et al., 2015).

Lineament detection algorithms vary considerably in approach. The earliest of these were developed for use with Landsat TM satellite imagery such as Edge Following and Graph Searching developed by Wang and Howarth (1990) and the Segment Tracing Algorithm (STA) by Koike et al. (1995). Algorithms used with potential field data, such as those by Lee et al. (2012) and Šilhavý et al. (2016), employ curvature and hillshade enhancements, respectively. Most recently, the LINDA software has been developed as a comprehensive tool for lineament detection for spectral and potential field data, and incorporates the STA algorithm Masoud and Koike (2017).

Object-Based Image Analysis (OBIA) is a powerful tool for analyzing spatially correlated groups of pixels. It utilises image segmentation algorithms to group contiguous pixels into image objects. The advantages of image objects are that the grouped pixels can be assessed together to measure texture and geometry and have corresponding summary statistics, whilst being linked geospatially through a topology (Lang, 2008). The generation of representative image objects is of paramount importance to OBIA and therefore some user knowledge is required for a successful analysis (Blaschke et al., 2004). The idea of user knowledge refining image objects is considered to be the change from an *object-based* workflow to an *object-oriented* workflow (Baatz et al., 2008). For simplicity, we retain the term *object-based* in this paper. Despite the adoption of OBIA techniques within the geosciences in the early 2000s, geological studies using OBIA techniques are largely restricted to classification studies (e.g. Grebby et al., 2016) and not to lineament detection. Previous studies using OBIA for lineament detection include Marpu et al. (2008), Mavrantza and Argialas (2008) and Rutzinger et al. (2007), who applied the method to Synthetic Aperture Radar (SAR), Landsat and LiDAR DTM data, respectively. The first application of the OBIA techniques to airborne geophysics was reported by Middleton et al. (2015) who utilised airborne magnetic data over the Enontekiö area of northern Finland.

The objective of this study is to develop semi-automated OBIA methods for geological lineament detection that integrate airborne geophysical and remote sensing datasets to create a composite lineament network. The top-down OBIA method from Middleton et al. (2015) is developed to integrate multiple datasets and compared to a new approach presented here which uses a bottom-up OBIA approach. The Southwest (SW) England region is used as a case study due to the complex structural geology and the availability of high-resolution airborne geophysical datasets. Final lineament maps are contrasted with a regional fault map from 1:50 000 British Geological Survey mapping districts in the study area.

1.1. The Southwest England region

The Tellus South West project (www.tellusgb.ac.uk) flew high-resolution regional airborne surveys over SW England, the coverage of which is outlined in Fig. 1. The geology of SW England provides an excellent opportunity to test OBIA methods to detect lineaments in a region where the structural geology is well-documented at multiple scales. The temperate climate of SW England limits well-exposed areas to coastal wave-cut platforms. Therefore, detailed structural studies are focussed along coastal sections and accurate field mapping inland is problematic due to soil cover. The high-resolution regional airborne geophysical surveys provide an excellent dataset for detection of geological lineaments. SW England is one of the most prospective areas within the UK for both metalliferous and industrial minerals and deep geothermal energy. The occurrence and exploitation of these resources are strongly influenced by regional fault networks and detailed lineament maps will help inform future exploration activity.

1.1.1. Previous lineament studies in SW England

Early attempts at regional lineament detection in SW England were conducted on Landsat MSS data (Moore and Camm, 1982). The study aimed to identify major structural lineaments relating to tin-tungsten mineralisation. Due to the coarse resolution of the imagery, the observations were only appropriate for 1:500 000 scale mapping, although significant NW-SE structures were clearly identifiable. A further study was conducted by James and Moore (1985) to investigate the temporal variations between different scenes and the incorporation of eastward-looking SAR data from Seasat imagery to enhance structural lineaments - although spatial resolution remained low.

Regional lineament detection using Landsat TM satellite imagery was first attempted by Smithurst (1990) and demonstrated good agreement with mapped major structures. A more detailed study by Rogers (1997) used two Landsat TM scenes which were reprocessed to 150 m pixels and applied four directional filters (N, E, NE, SE). Lineaments were manually digitised based on four criteria: a width/length ratio >0.5; within ± 30° of the directional filter; be larger than four pixels; a qualitative strike length significance (Rogers, 1997). The study was effective but was hindered by cloud cover and rejected lineaments <4 pixels long, therefore neglecting significant structures <600 m in length.

A more recent study mapping strike-slip faults along the north Cornwall coast at Westward Ho! demonstrated that, in well-exposed areas, rapid structural mapping from aerial photography is a valuable approach (Nixon et al., 2011).

1.1.2. Geological setting

The bedrock geology of SW England comprises Devonian-Carboniferous sedimentary rocks, metamorphosed to sub-greenschist facies during the Variscan Orogeny and intruded by a Permian granite batholith (Fig. 1). The sedimentary successions were deposited in six E-W-trending extensional basins which were subsequently inverted during the Variscan Orogeny (Leveridge and Hartley, 2006). The Variscan Orogeny resulted in two phases of NNW-directed thrusting which formed an ENE-WSW to E-W-trending fault system (Alexander and Shail, 1995, 1996; Leveridge et al., 2002; Leveridge and Hartley, 2006). Steeply-dipping NW-SE and subordinate NNE-SSW strike-slip faults (Dearman, 1963) developed during the Variscan collision (Leveridge et al., 2002); some NW-SE faults may have been inherited from the pre-Variscan extensional regime (Roberts et al., 1993; Shail and Leveridge, 2009).

The batholith was emplaced in an Early Permian post-orogenic extensional setting and the exposed plutons have a spatial correlation with major NW-SE faults (Dearman, 1963; Alexander and Shail, 1996). The extensional reactivation of ENE-WSW to E-W striking Varsican thrusts was accompanied by the creation of new steeply-dipping conjugate extensional faults, that often host granite-related W-Sn-Cu mineralisation, and was followed by minor Permian intraplate shortening episodes (Shail and Alexander, 1997). Subsequent latest Permian to Triassic ENE-WSW extension reactivated older NW-SE faults and created new NW-SE to N-S faults, “cross-courses”, that cut earlier granite-related mineralisation and locally host epithermal basinal brine mineralisation (Scrivener et al., 1994; Shail and Alexander, 1997). The regional fracture network had essentially formed by the late Triassic. However, several major NW-SE faults in the east of the region underwent Oligocene sinistral reactivation to form pull-apart basins (Holloway and Chadwick, 1986; Gayer and Cornford, 1992) and their infill is locally deformed in a presumed Miocene dextral strike-slip regime (Holloway and Chadwick, 1986).

Whilst the structural evolution, and development of regional fault networks in SW England is complex, the dominant structural trends are ENE-WSW to E-W and NW-SE with subordinate NE-SW and N-S elements.

2. Materials and methods

The airborne geophysical data used in this study were selected to demonstrate the strength of the method for integrating multiple datasets to produce a composite lineament network. The methods herein describe data pre-processing steps and analysis in eCogntion software (v9.3, Trimble, Germany). Post-processing was also necessary for quality assessment of the data and to create and manipulate metadata. Full details of the software used in these steps can be found in the Supplementary Information (S1). The two OBIA methods presented here can be downloaded individually as an eCognition Rule Set from the University of Exeter at http://empslocal.ex.ac.uk/obld2.

2.1. Airborne geophysical datasets

Data from the Tellus South West project provide a new opportunity to accurately determine lineaments at high resolution across SW England. The airborne data were acquired in two surveys; the LiDAR data collected in summer 2013 and the magnetic and radiometric data in late 2013 to early 2014 (Beamish and White, 2014). The surveys have near-complete coverage, except for an inset of data within the magnetic and radiometric data which was not collected over the Tamar Estuary at Her Majesty's Naval Base (HMNB) Devonport (Fig. 1).

The magnetic and radiometric data were collected simultaneously by CGG Airborne Survey (Pty). Final quality assurance and quality control of the data were undertaken by the British Geological Survey (Beamish and White, 2014). The data were gridded using a minimum-curvature algorithm and supplied at a pixel resolution of 40 m. The survey parameters are summarised in Table 1. In this study, the Total Magnetic Intensity (TMI) from the magnetic data (corrected using the International Geomagnetic Reference Field) and the Total Count channel from the radiometric data were used.

The LiDAR data were collected as part of a separate survey at 1 point/metre^2 with 25 cm vertical accuracy. The data were acquired by the British Antarctic Survey, processed by Geomatics (Environment

Table 1
Survey parameters for the Tellus South West airborne geophysical survey compiled from Beamish and White (2014) and Gerard (2014). The separate LiDAR survey flew an ENE-WSW angle to align with the axis of the peninsula to the west.

Survey Parameter	Magnetic	Radiometric	LiDAR
Line Spacing	200 m	200 m	700 m
Line Orientation	N-S	N-S	E-W and ENE-WSW
Tie Lines	2000 m	2000 m	N/A
Average Altitude	91.55 m	91.55 m	1100 m
Speed	71.21 m/s	71.21 m/s	Unknown
Sample Frequency	20 Hz	1 Hz	1 point/m^2

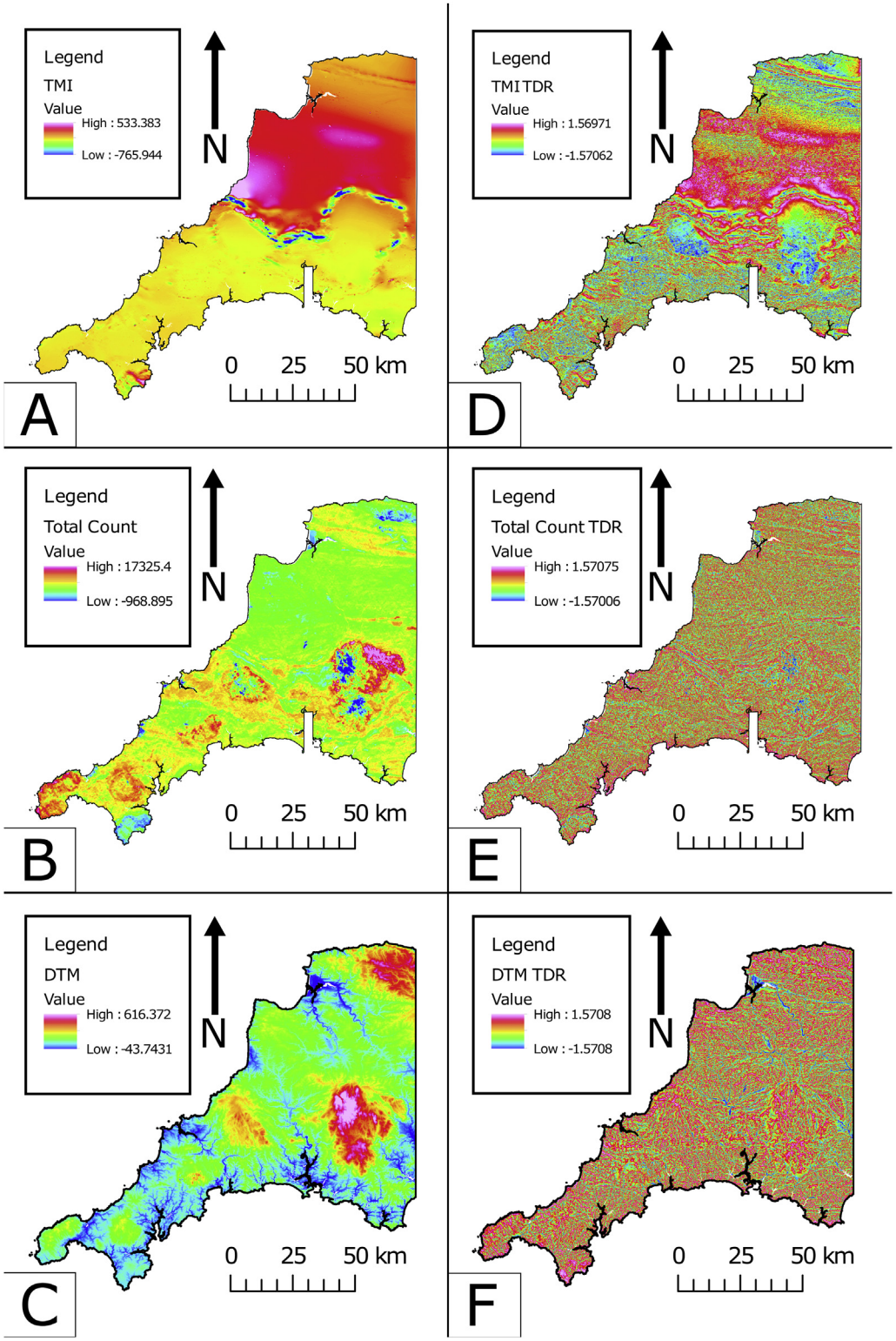

Fig. 2. Input data from Tellus South West (A) magnetic data in TMI; (B) radiometric data in Total Count; (C) LiDAR DTM data in metres; (D) TDR-transformed magnetic data; (E) TDR-transformed radiometric data; (F) TDR-transformed LiDAR DTM data.

Agency), and overseen by the Centre for Ecology and Hydrology (CEH). Some areas of low quality data acquisition exist in urban areas and dense vegetation (Gerard, 2014). The data were supplied in raster format as a DTM with a pixel resolution of 1 m, and are used here under an Open Government Licence (Ferraccioli et al., 2014).

The initial airborne geophysical data from the Tellus South West project are illustrated in Fig. 2A–C. The three datasets each add different information to the analysis. The LiDAR data captures lineaments that are manifest in the geomorphology of the region. Lineaments derived from magnetic data may indicate the presence of geological structure extending at depth in the crust. The radiometric data, specifically the Total Count channel used here, senses lineaments that may have acted as fluid conduits resulting in mineral alteration. Lower values therefore represent the leaching of radiogenic elements such as

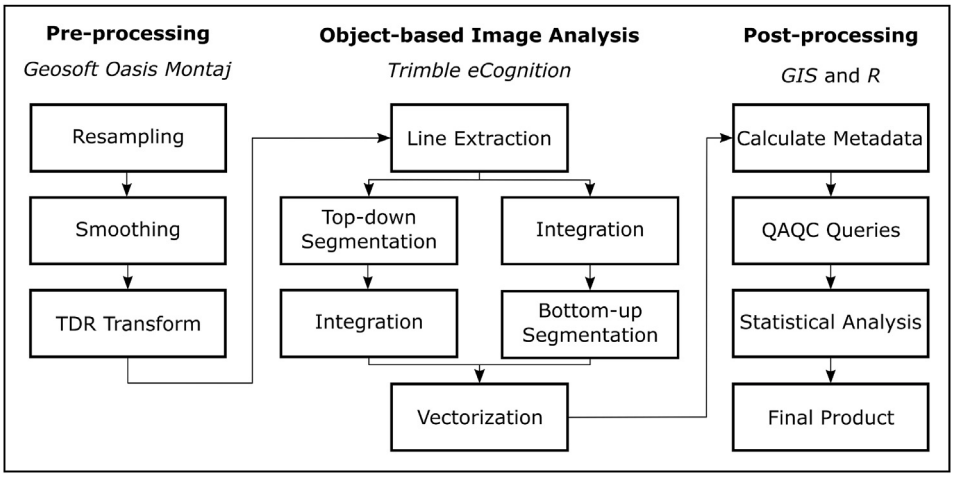

Fig. 3. Workflow for creating a lineament network using both OBIA methodologies. The split in the flowchart indicates the slightly different path for each method rather than parallelised analysis.

potassium and uranium.

2.2. Lineament Detection

The two different OBIA methods described here represent a novel approach to geological lineament detection where airborne geophysical and remote sensing datasets can be integrated in order to produce a comprehensive and composite lineament network. The methods primarily use the eCognition software (v9.3, Trimble, Germany) and the Cognitive Network Language (CNL). The CNL provides a variety of tools for OBIA workflows. The workflow for the two stand-alone OBIA methodologies using top-down and bottom-up segmentation techniques is summarised in Fig. 3.

2.2.1. Pre-processing

Initial pre-processing was conducted in *R* project software (https://cran.r-project.org) using the *raster* package (v2.6-7, Hijmans et al., 2017). All datasets were resampled to the same extent and resolution (40 m pixels) using a bidirectional operator before being clipped to the coastline. The dashed rectangular area missing in the magnetic and radiometric data over HMNB Devonport was not removed from the LiDAR data (Fig. 1).

The magnetic and LiDAR data underwent further preprocessing steps in the Oasis Montaj programme (v8.5, Geosoft, Canada) to remove noise. These include cultural artefacts relating to buildings and infrastructure as well as minor corrugations across flight lines. A smoothing algorithm was applied in Oasis Montaj to mitigate the artefacts from densely vegetated and urbanised areas in the LiDAR DTM. As a result, the topographic expression of anthropogenic features such as road cuttings were drastically reduced and smoothed. The smoothed product was carefully compared to the original data to ensure minimal loss of geological information.

The final pre-processing step applies the TDR function to enhance the continuity of the data (Equation (1)).

$$TDR = \tan^{-1}\left(\frac{\frac{\partial T}{\partial z}}{\sqrt{\left(\frac{\partial T}{\partial x}\right)^2 + \left(\frac{\partial T}{\partial y}\right)^2}}\right) \quad (1)$$

The TDR transform uses the arctangent of the ratio of vertical derivative to total horizontal derivative and therefore normalizes the data to the range $\pi/2$ to $-\pi/2$ (Miller and Singh, 1994). The normalization allows comparison of the data and the ratio of the derivatives acts as a gain control to ensure minor gradient changes are not lost (Verduzco et al., 2004). The TDR transform is applied to all three datasets, illustrated in Fig. 2D–F. For the DTM and Total Count data, the vertical derivative is calculated using convolution rather than Fourier transform.

The TDR transform is commonly used to identify the edges of isolated magnetic bodies at the zero contour of the transformed data (Fairhead et al., 2004; Beamish and White, 2011; White and Beamish, 2011). The TDR transform is applied here to search for minima; these are considered an effective proxy for lineaments related to fault zones. It is assumed the minima are generated through preferential erosion (LiDAR DTM), breakdown of magnetic minerals (magnetic data) or leaching of radioelements (radiometric data). It is acknowledged that in some geological environments lineaments may be represented by maxima (indurated rocks or magnetic and radiometric highs). Some knowledge of the geology is key to deciding whether to search for minima or maxima, or both. Full details of the pre-processing steps can be found in the Supplementary Information (S2).

2.2.2. Line extraction

The *line extraction* algorithm in the CNL was used to create a newly derived lineness raster from each input dataset. The algorithm uses a user-defined, rectangular kernel filter to assess the similarity of pixels. The kernel was set to search at regular interval angles of 5°. The parameters for line extraction were optimised to be the same across all datasets to produce three lineness rasters with similar attributes that could be subsequently integrated. The resultant raster has a range of 0–255; higher values indicate a higher probability that a lineament exists. A detailed description of the algorithm within eCognition is provided in the Supplementary Information (S1).

2.2.3. Top-down segmentation

A top-down methodology involves the segmentation of an image into smaller and smaller objects and the downward propagation of object levels in the CNL (Diamant, 2004). Determining object relationships across different levels such as super-objects is advantageous for manipulating specific parts of the original object (such as the end) and is used in this instance to preferentially grow objects at their ends.

Lineament detection through a top-down segmentation was achieved using the *multi-threshold segmentation* and *chessboard segmentation* tools in the CNL. The workflow is based on the Object-Based Lineament Detection (OBLD) algorithm of Middleton et al. (2015), which is further developed here to integrate all three input datasets to create a composite lineament network. The OBLD algorithm is discussed in full within Middleton et al. (2015).

The general workflow for lineament detection using top-down OBIA methods from multiple datasets is summarised in Fig. 3. The

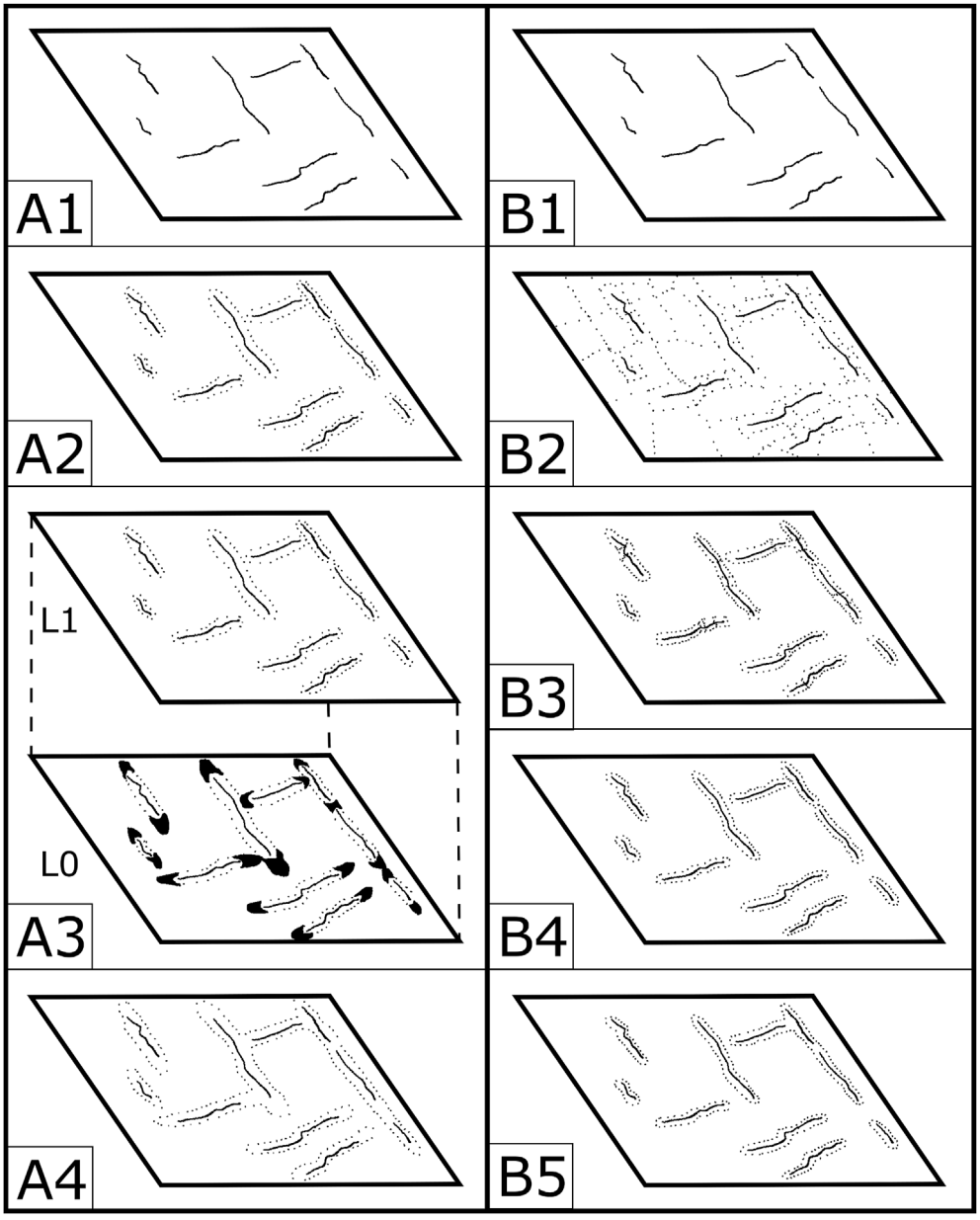

Fig. 4. Segmentation methods for each OBIA approach. (A) Illustrates the top-down method where 1 = the lineness raster; 2 = multi-theshold segmentation; 3 = extension through sub-levels, chessboard segementation and super-objects; 4 = object merging. (B) Illustrates the bottom-up method where 1 = the lineness raster; 2 = multi-resolution segmentation; 3 = spectral difference merging; 4 = border assessment; 5 = object merging.

segmentation steps and use of object-levels for extending objects are illustrated in Fig. 4A1-4.

The integration steps developed here for the top-down OBIA method involve the merging of separate image object sets from each dataset. A complementary merged lineness raster is created by summing the individual lineness rasters and normalising to 0–255. Objects are extended in a similar fashion using a new sub-level (L0) under the existing data, as is the case in Middleton et al. (2015), and further segmented using the *chessboard segmentation* tool. However, in this step, extensions are determined from the merged lineness raster and therefore could be based on values derived from a different dataset. An additional requirement is that object-ends are only extended if in proximity to another object-end. A final cleaning step removes any spurious objects that are below a given area or asymmetry threshold.

2.2.4. Bottom-up segmentation

The bottom-up method for lineament detection involves the segmentation of the whole image, using the *multi-resolution segmentation* tool, into many, differently sized, objects which are subsequently merged (Dragut et al., 2010; Eisank et al., 2014). Merging can be based on spectral, statistical, textural or geometric properties and is highly versatile.

The integration step occurs prior to segmentation in the bottom-up method. As before, a composite lineness raster is created by summing the lineness rasters and normalising to 0–255. Fig. 4B1-5 illustrates how the composite lineness raster is segmented using the *multi-resolution segmentation* algorithm and the subsequent merging of objects using the *spectral difference* algorithm. Next, the resulting objects are then classified based on the mean pixel value in the lineness raster into major and minor lineaments according to a threshold defined by the user. The threshold is defined heuristically based on user knowledge of the region, and is thus case-specific.

Major and minor lineaments are refined using a border assessment to merge segments of a lineament which may contain both major and

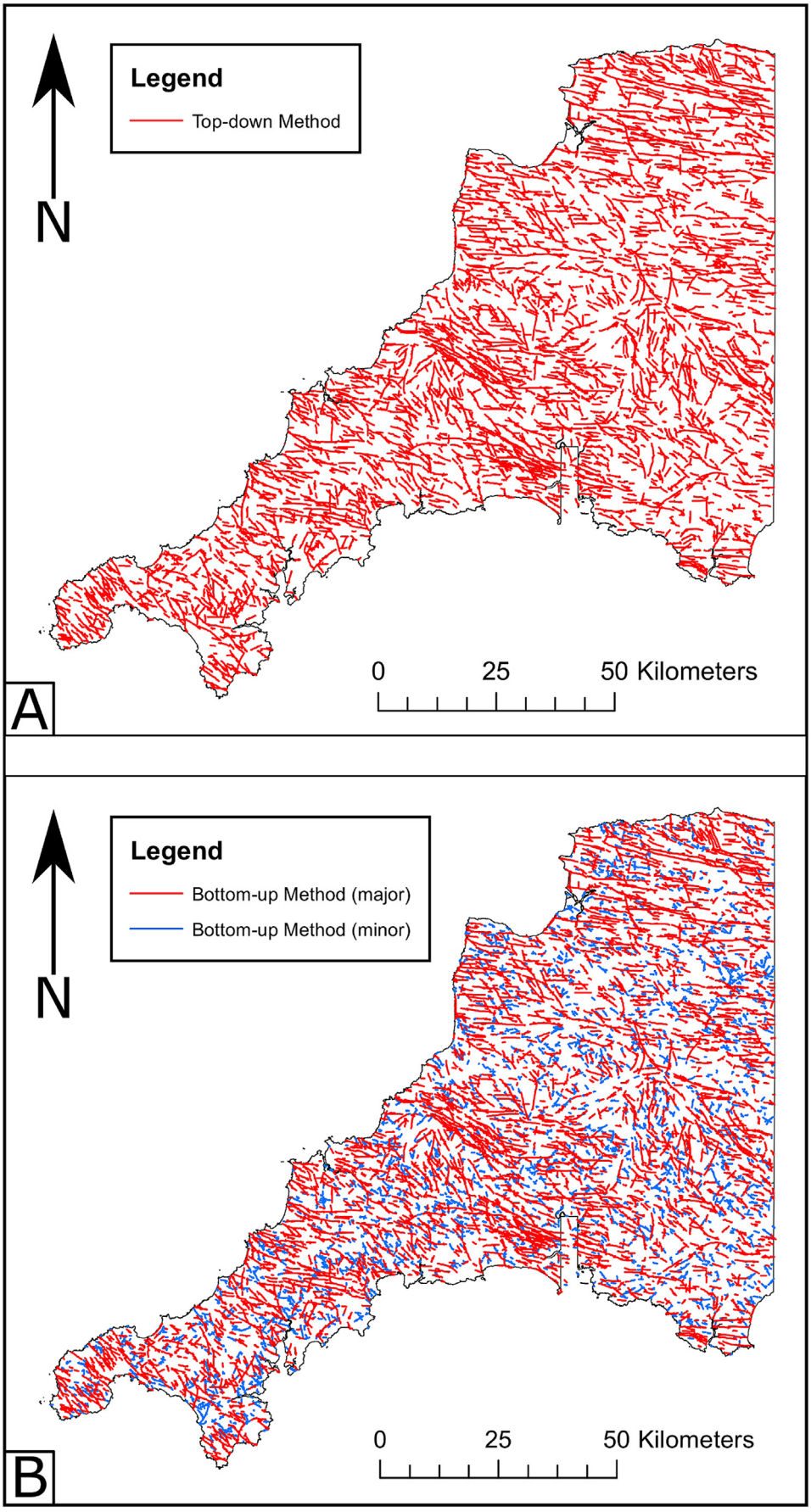

(caption on next page)

Fig. 5. Final regional lineament maps for the (A) top-down and (B) bottom-up methodologies. The bottom-up dataset is represented as major and minor lineaments based on the metadata. Black lines represent the coast, rectangular inset area of HMNB Devonport and the eastern limit of the study area. This figure includes OS data © Crown Copyright and database right (2018).

minor components into a continuous object set of either major or minor objects. Initially, major lineament objects are expanded by one pixel to minimise single pixel borders with minor lineament objects. Minor lineament objects which have the majority (60%) of their relative border in contact with major objects are converted into major lineament objects. Major lineament objects are shrunk by growing unclassified objects into the major object where the composite lineness raster is below the heuristically defined threshold for a major lineament. The remaining major lineament objects are then merged. Major objects are converted into minor objects where the majority (60%) of the relative border is in contact with a minor lineament. Cleaning steps remove objects with an area below a given threshold (in this case 50 pixels for major, and 30 pixels for minor lineaments) and also remove pixels at the edges of objects below a threshold in the composite lineness raster; this is tailored to major and minor objects.

2.2.5. Vectorization and metadata

The final step using the CNL was to convert objects to polylines and export these to a shapefile with the corresponding metadata. The polylines were vectorized into skeleton polylines of the objects they represent. Skeleton polylines are most efficient at capturing objects that represents a complex lineament network.

The metadata for the top-down segmentation method includes binary fields detailing the source dataset for each lineament (extension, LiDAR DTM, magnetic, radiometric). The end-user can manipulate these fields to fully describe the source data for the lineament. For the bottom-up segmentation method, metadata was restricted to the classes of either major or minor lineaments.

2.2.6. Post-processing

Post-processing of the metadata involved the calculation of the orientation and length of polylines and was conducted in the ESRI ArcGIS software. The computed polyline length, orientation and a direction (N, NE, E, or SE) were included in the metadata of the vector file.

The polyline data for both top-down and bottom-up methods were interrogated through database queries in the GIS. The data from the top-down method were found to have 29 artefact polylines associated with the extension step of the method. These artefacts, defined as disconnected polylines with lengths < 40 m, were removed from the final lineament dataset. Full details of the post-processing steps can be found in the Supplementary Information (S3).

3. Results

The polyline data for both top-down and bottom-up methods were assessed for line length and orientation. A qualitative analysis of the data is presented, as well as a comparison with the existing regional map compiled from the 1:50 000 DiGMap data from the British Geological Survey. The polyline output for the top-down and bottom-up methods are presented in Fig. 5.

3.1. Statistical analysis

Summary statistics for each polyline dataset are presented in Table 2 and are graphically displayed using boxplots (Fig. 6) and half-rose diagrams (Fig. 7) for polyline lengths and orientations, respectively. It is apparent from Table 2 that the mean polyline lengths are significantly skewed by outlying data in both datasets. Therefore, the median is considered a more appropriate measure of average polyline length. Due to the positively skewed distribution, the interquartile range, demarcated by the box in Fig. 6 is used to reflect the dispersion within each dataset. The bottom-up method shows less dispersion compared to the top-down method indicating a more consistent polyline length. Nevertheless, the top-down method produces a longer median polyline length.

Table 2
Summary statistics for the polyline length (in metres) of each datasets. The mean is not considered a representative centre value due to the high skew. The range, median and kurtosis describe the non-normal distribution whilst the IQR provides a better comparison of dispersion than standard deviation. SD = standard deviation, IQR = Interquartile Range. The datasets are denoted as TD (top-down) and BU (bottom-up) where the numbers 8 and 16 refer to the number of compass directions used in post-processing.

	Mean	SD	Median	Range	Skew	Kurtosis	IQR
TD16	360.58	491.83	191.05	8700.06	4.09	27.24	289.93
TD8	483.09	678.27	238.54	10613.90	4.09	27.45	429.84
BU16	248.34	346.15	143.95	7706.14	5.82	58.47	183.48
BU8	327.87	470.13	180.28	8632.71	5.17	44.12	261.45

The distribution of orientation is presented as half-rose diagrams in Fig. 7. It is apparent from the rose diagrams that both methods capture a similar trend in the orientation of lineaments. The dominant trends range from E through to SE with subordinate NE and N-S trends. Between the two methods there is little difference in the overall distribution, although, the top-down method appears to emphasise SE-trending lineaments more than the bottom-up method.

4. Discussion

Two stand-alone OBIA methods for integrated lineament detection have been presented. Both methods can create similar data products but include different metadata which are further enhanced to include lineament length and orientation during post-processing. The initial use of line extraction in the CNL demonstrated by Middleton et al. (2015) is effective, especially where the TDR transform is applied to airborne magnetic data. This study extends the use of OBIA methods to TDR-transformed Total Count channel from airborne radiometric data and elevation data from an airborne LiDAR DTM.

4.1. Application of the Tilt Derivative

Image analysis often requires an effective enhancement to extract detailed information from an input dataset. The TDR transform has previously been applied for edge detection where the zero-contour corresponds to the edge of magnetic bodies and where the signal does not overlap with nearby sources (Fairhead et al., 2004; Beamish and White, 2011; White and Beamish, 2011).

The use of TDR minima for detecting weakness zones in the bedrock, such as shear zones or fault zones, was described for worming techniques by Airo and Leväniemi (2012). The selection of using minima does not preclude the use of maxima and can be adapted for geological environments where fault zones may have enhanced magnetic, radiogenic or hardness properties. The detection of geological lineaments from TDR minima of airborne magnetic data using OBIA methods was first applied by Middleton et al. (2015) and compared to a similar worming technique to that of Airo and Leväniemi (2012). Middleton et al. (2015) also applied to the TDR transform to airborne LiDAR DTM data but did not incorporate it into the semi-automated analysis.

Here, the TDR transform has been successfully applied to airborne magnetic and LiDAR DTM, in addition to the Total Count channel of

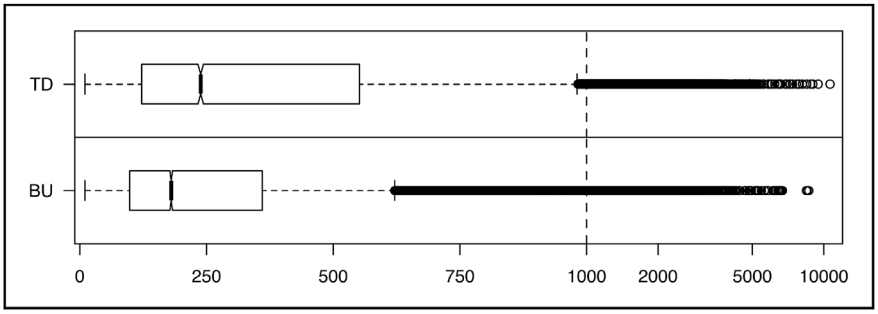

Fig. 6. Boxplots illustrating the variations in polyline lengths (in metres) for the top-down (TD) and bottom-up (BU) methods. The TD method demonstrates a broad spread of the interquartile range and superior polyline lengths, whereas the BU method produces shorter lengths and has a smaller interquartile range.

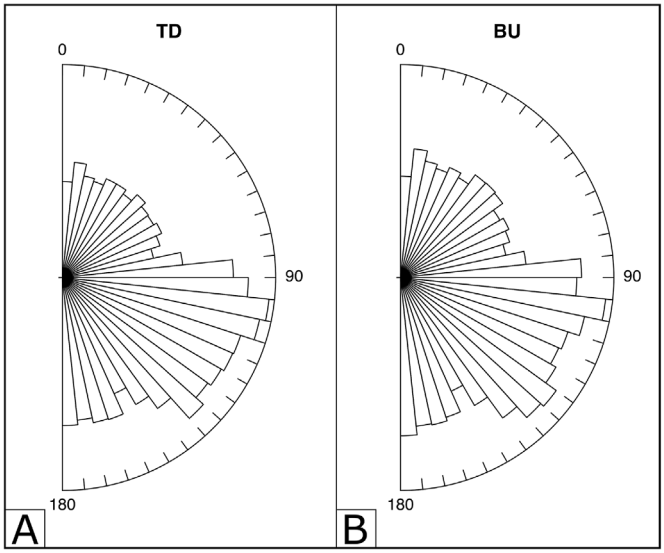

Fig. 7. Half-rose plots representing the population of polyline angles for top-down (TD) and bottom-up (BU) datasets. The data are binned at 6° angles. Both methods capture the same global trends with dominant populations trending ESE and SE with subordinate S populations.

airborne radiometric data. It is necessary to calculate the vertical derivative for the TDR transform using convolution, rather than a Fourier transform, for the LiDAR DTM and Total Count data. The resulting composite lineament networks are the first to use the TDR transform in this manner, and to successfully integrate multi-sourced data into a semi-automated analysis for geological lineament detection.

4.2. Top-down vs. Bottom-up segmentation

Top-down OBIA methods for geological lineament detection are effective at capturing the regional lineament network. The method does require user knowledge to define appropriate thresholds for segmentation, although these can be readily determined through a heuristic approach. Extending objects is computationally intensive and adds significant processing time to the top-down method. Furthermore, assigning object-ends from super-objects in a sub-level results in only two nodes for extension, which can be problematic for multi-branched objects. Additional extension after integrating objects is more sensitive as it requires another object-end to exist within proximity to that being extended. There is also no control over the direction of growth. Finally, the output metadata provides information on the data source of the lineament, which can be useful for geological interpretation.

In contrast, the bottom-up OBIA methodology requires less user knowledge since the whole image is segmented and then merged objectively. The method takes a slightly different approach by integrating the different lineness rasters into a composite lineness raster prior to segmentation. It also uses a border assessment approach to merge major objects into more extensive structures where they are interspersed with minor objects and create more robust lineaments. Some information is lost though integrating the lineness rasters, however, this, coupled with the border assessment step, makes the bottom-up method much more computationally efficient compared to top-down methods. Although some detail is lost during integration, metadata can be produced by defining thresholds for major and minor lineament classes.

4.3. Comparison with existing geological mapping

Previous regional maps are often compiled for specific projects and tailored to focus on specific faults. The most complete regional map can be compiled from the 1:50 000 DiGMap data from the British Geological Survey (Fig. 8). This map incorporates fault data from thirty mapping districts in the region that was originally mapped at 1:10 000 scale in the field and later collated and reduced to 1:50 000.

The regional 1:50 000 fault map is markedly inconsistent. Some districts have a high density of faults (Chulmleigh), whereas others are nearly completely devoid of them (Bodmin and Ivybridge). The poor outcrop exposure inland invariably makes conventional geological mapping difficult. However, regional variability is also influenced by lithostratigraphy (recognition of fault separation and geomorphological features for which Chulmleigh has a very favourable lithostratigraphy) and changes in historical emphasis and mapping techniques (data for the Bodmin and Ivybridge were acquired over a century ago). Faults in upland granite areas are generally under-represented.

The lineament datasets created from OBIA methods (Fig. 5) are more comprehensive and consistent than the existing regional fault map (Fig. 8). Furthermore, lineaments generated capture similar, but more distinct, structural trends. OBIA lineaments are comparatively shorter in length, although they have not been subjected to cartographic drafting as is the case with the 1:50 000 data.

4.4. Assessment of the final lineament networks

The final lineament maps presented in Fig. 5 demonstrate two stand-alone OBIA methods for detecting lineaments. Both methods provide comprehensive and consistent lineament maps which are created semi-automatically with minimal prior knowledge by the user. By integrating data from multiple sources, a composite lineament network is created based on geophysical, geological and geomorphological properties.

The results from the two OBIA methods produce similar overall lineament patterns despite their fundamental differences. The extracted lineament networks are therefore considered to be robust and an accurate representation of the regional geological structure. Statistical analysis of the orientation of lineaments from both methods concur with the trends recorded from field studies by Alexander and Shail (1995, 1996); Leveridge et al. (2002); Leveridge and Hartley (2006); Hughes et al. (2009); Nixon et al. (2011).

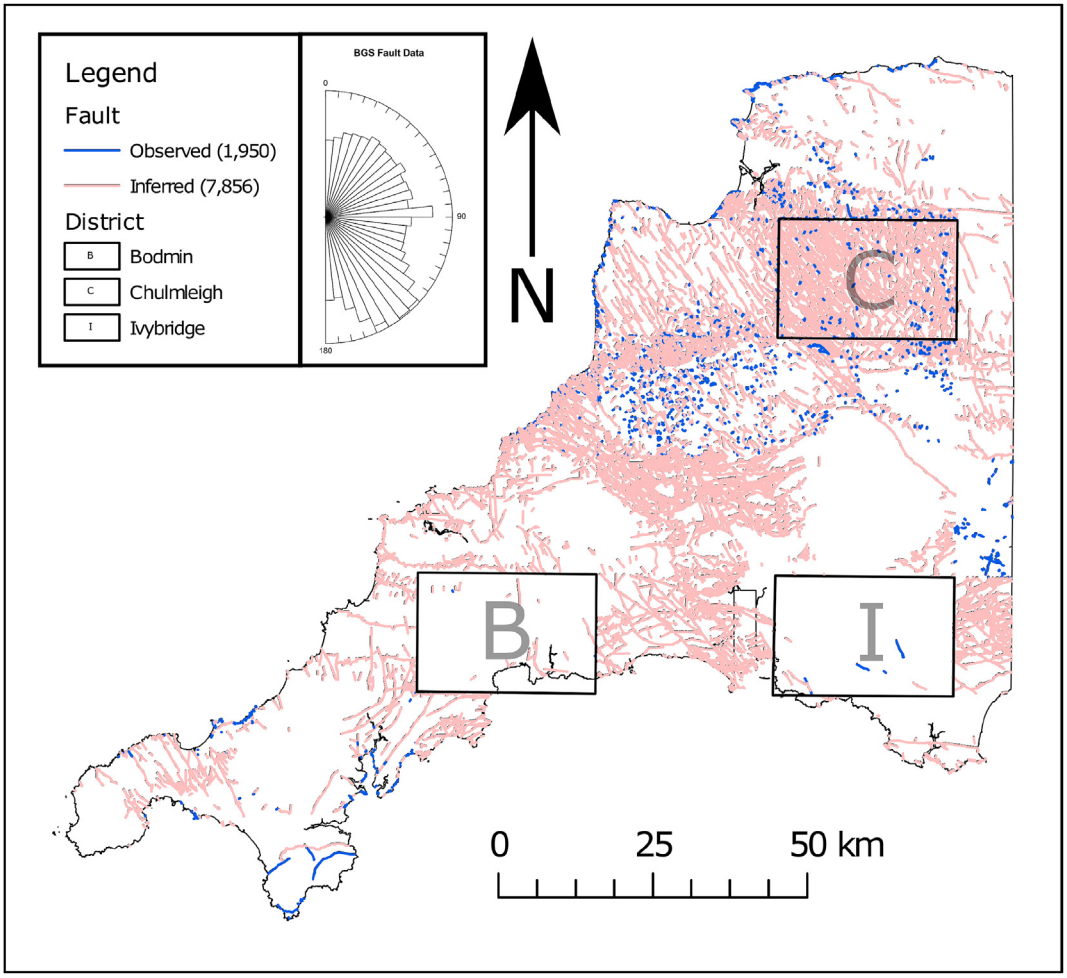

Fig. 8. The BGS 1:50 000 linear data for faults in SW England. All faults have been grouped into observed or inferred with the number of objects noted in the legend. It is apparent that much of the BGS linework is based on inferred faults which are a likely combination of both geological and geomorphological information resulting in longer interpreted lengths than observed faults. The map also illustrates the inconsistencies across different mapping districts such as Chulmleigh (C), Ivybridge (I) and Bodmin (B). Furthermore, an inset is included to illustrate the orientation of all mapped (observed and inferred) faults. This figure is based on BGS 1:625 000 digital data and includes OS data ©Crown Copyright and database right (2018).

Previous attempts at using OBIA methods for lineament detection have only been applied to a single input dataset. These include application to SAR (Marpu et al., 2008), Landsat (Mavrantza and Argialas, 2008) and LiDAR DTM data (Rutzinger et al., 2007), which restricts the mapping to lineaments that are only present at surface. Conversely, Middleton et al. (2015) use airborne magnetic data to determine whether lineaments are related to structures present in the deeper crust. The OBIA methods developed here are the first to integrate three multi-sourced input datasets for both surficial and subsurface lineament detection to create a more comprehensive, composite lineament network.

The two contrasting OBIA methods presented here have different applications. For regional datasets, both methods can create a semi-automated lineament map. However, the bottom-up method provides a computationally efficient lineament map which sacrifices polyline lengths and output metadata. The metadata from the top-down method provides useful information on whether a lineament has a geomorphological expression (LiDAR DTM), may pertain to a deeper structure (magnetic data) or have been leached during alteration (radiometric data). Where a lineament has been detected in all three datasets, it is considered that this is more certain and likely to significant. Irrespective of the OBIA method selected, the common pre- and post-processing steps are crucial to ensuring quality of the final lineament maps. Careful pre-processing can mitigate the effect of artefacts in the input data, whereas thorough post-processing will remove any spurious lineaments generated during detection.

There is, of course, scope to develop an algorithm that finds a better middle ground between the two OBIA methodologies. Revised methods could attempt to optimise lineament lengths for the bottom-up method or reduce computational time of the top-down method.

5. Conclusions

Two stand-alone OBIA methods for the detection of geological lineaments from airborne geophysics and remote sensing datasets, to create a composite lineament network, are presented. OBIA methods for lineament detection are highly effective and can make use of top-down and bottom-up segmentation techniques.

The use of the TDR transform, and the assumption that lineaments are represented by minima in the magnetic, radiometric and LiDAR DTM data, is valid for the detection of geological lineaments in SW England, but does not preclude the algorithm from detecting maxima where appropriate. By applying the TDR transform to radiometric Total Count and LiDAR DTM data using convolution to calculate the vertical derivative, comparable datasets can be produced with similar properties for lineament detection.

The further development of a top-down OBIA method for geological lineament detection allows the effective integration of multi-sourced datasets. The newly developed bottom-up OBIA method provides a

more computationally efficient means of detecting lineaments across multiple datasets with less user input required at the expense of lineament length. Both OBIA methods produce similar composite lineament networks, which capture the orientations of existing mapped structures, and are therefore considered to be a robust representation of the regional structural geology.

By integrating data from multiple sources, a comprehensive and composite lineament network is created based on geophysical, geological and geomorphological properties. The top-down method provides metadata that can aid geological interpretation and help determine the certainty and significance of a lineament. The bottom-up method is more computationally efficient but produces shorter lineament lengths and less detailed metadata.

Acknowledgements

We would like to thank three anonymous reviewers for comments that have improved this manuscript. The work was completed as part of doctoral research by CMY funded by the British Geological Survey (BGS) (S267) and the Natural Environment Research Council (NERC)GW4+ Doctoral Training Partnership (NE/L002434/1) in collaboration with the Geological Survey of Finland (GTK). Data used in this study are available from the Tellus South West project website (www.tellusgb.ac.uk). CMY is grateful to Eija Hyvönen (GTK) who advised on data preparation, and gave her time and computer facilities whilst CMY visited Rovaniemi, Finland. We are grateful to Jim White (BGS) for providing initial training in the Geosoft Oasis Montaj software and his constructive comments on an early draft of this manuscript. This paper is published with the permission of the Executive Director, British Geological Survey (UKRI).

Appendix A. Supplementary data

Supplementary data to this article can be found online at https://doi.org/10.1016/j.cageo.2018.11.005.

References

Airo, M.-L., Leväniemi, H., 2012. Geophysical structures with gold potential in southern Finland. In: Grönholm, S., Kärkkäinen, N. (Eds.), Gold in Southern Finland: Results of GTK Studies 1998-2011. Geological Survey of Finland, Special Paper 52. Geological Survey of Finland, pp. 227–244.

Airo, M.-L., Wennerström, M., jun 2010. Application of regional aeromagnetic data in targeting detailed fracture zones. J. Appl. Geophys. 71 (2–3), 62–70. http://linkinghub.elsevier.com/retrieve/pii/S0926985110000388.

Alexander, A.C., Shail, R.K., 1995. Late Variscan structures on the coast between Perranporth and St. Ives, Cornwall. Proc. Ussher Soc. 8, 398–404.

Alexander, A.C., Shail, R.K., 1996. Late- to post-Variscan structures on the coast between Penzance and Pentewan, south Cornwall. Proc. Ussher Soc. 9, 72–78.

Baatz, M., Hoffmann, C., Willhauck, G., 2008. Progressing from object-based to object-oriented image analysis. In: Blaschke, T., Lang, S., Hay, G.J. (Eds.), Object-based Image Analysis: Spatial Concepts for Knowledge-driven Remote Sensing Applications. Springer-Verlag, Berlin, pp. 29–42.

Beamish, D., White, J., 2014. TellusSW: Airborne Geophysical Data and Processing Report. Tech. rep., British Geological Survey Open Report, OR/14/014.

Beamish, D., White, J.C., 2011. Aeromagnetic data in the UK: a study of the information content of baseline and modern surveys across Anglesey, North Wales. Geophys. J. Int. 184 (1), 171–190.

Blakely, R.J., Simpson, R.W., 1986. Approximating edges of source bodies from magnetic or gravity anomalies. Geophysics 51 (7), 1494.

Blaschke, T., Burnett, C., Pekkarinen, A., 2004. Image segmentation methods for object-based analysis and classification. In: de Jong, S.M., van der Meer, F.D. (Eds.), Remote Sensing Image Analysis: Including the Spatial Domain. Springer Netherlands, pp. 211–236.

Dearman, W.R., 1963. Wrench-faulting in Cornwall and South Devon. PGA (Proc. Geol. Assoc.) 74 (3), 265–287.

Debeglia, N., Martelet, G., Perrin, J., Truffert, C., Ledru, P., Tourlie, B., aug 2006. Semi-automated structural analysis of high resolution magnetic and gamma-ray spectrometry airborne surveys. J. Appl. Geophys. 58 (1), 13–28. http://linkinghub.elsevier.com/retrieve/pii/S0926985105000273.

Diamant, E., 2004. Top-down unsupervised image segmentation (it sounds like an oxymoron, but it actually isn't). In: Proceedings of the 3rd Pattern Recognition in Remote Sensing Workshop (PRRS'04), August 2004. Kingston University, UK.

Dragut, L., Tiede, D., Levick, S.R., 2010. ESP: a tool to estimate scale parameter for multiresolution image segmentation of remotely sensed data. Int. J. Geogr. Inf. Sci. 24 (6), 859–871.

Eisank, C., Smith, M., Hillier, J., 2014. Assessment of multiresolution segmentation for delimiting drumlins in digital elevation models. Geomorphology 214, 452–464.

Fairhead, J.D., Green, M., Verduzco, B., Mackenzie, C., 2004. A new set of magnetic field derivatives for mapping mineral prospects. In: ASEG Extended Abstracts, vol. 1. pp. 1.

Ferraccioli, F., Gerard, F., Robinson, C., Jordan, T., Biszczuk, M., Ireland, L., Beasley, M., Vidamour, A., Barker, A., Arnold, R., Dinn, M., Fox, A., Howard, A., 2014. LiDAR Based Digital Terrain Model (DTM) Data for South West England.

Gayer, R.A., Cornford, C., 1992. The Portledge-Peppercombe Permian outlier. Proc. Ussher Soc. 8, 15–18.

Gerard, F., 2014. LIDAR QUALITY CONTROL REPORT Project: PM 1478. Tech. rep., Geomatics. Environment Agency, National Operations.

Grebby, S., Cunningham, D., Naden, J., Tansey, K., 2012. Application of airborne LiDAR data and airborne multispectral imagery to structural mapping of the upper section of the Troodos ophiolite, Cyprus. Int. J. Earth Sci. 101, 1645–1660.

Grebby, S., Field, E., Tansey, K., 2016. Evaluating the use of an object-based approach to lithological mapping in vegetated terrain. Rem. Sens. 8 (10), 843. http://www.mdpi.com/2072-4292/8/10/843.

Hijmans, R.J., van Etten, J., Cheng, J., Mattiuzzi, M., Sumner, M., Greenberg, J.A., Perpinan Lamigueiro, O., Bevan, A., Racine, E.B., Shortridge, A., Ghosh, A., 2017. Raster: Geographic Analysis and Modeling with Raster Data. R Package, Version 2. pp. 6–7.

Holloway, S., Chadwick, R.A., 1986. The Sticklepath-Lustleigh fault zone: Tertiary sinistral reactivation of a Variscan dextral strike-slip fault. J. Geol. Soc. 143, 447–452 London.

Hughes, S.P., Stickland, R.J., Shail, R.K., LeBoutillier, N.G., Alexander, A.C., Thomas, M., 2009. The chronology and kinematics of Late Palaeozoic deformation in the NW contact metamorphic aureole of the Land's End Granite. Geosci. South-West England 12, 140–152.

James, J.M., Moore, J.M., 1985. Multi-seasonal imagery studies for geological mapping and prospecting in cultivated terrain of S.W. England. In: Fourth Thematic Conference: "Remote Sensing for Exploration Geology", San Francisco, California, April 1-4, 1985. April 1 - 4, 1985. San Francisco, California, pp. 475–484.

Koike, K., Nagano, S., Ohmi, M., 1995. Lineament analysis of satellite images using a Segment Tracing Algorithm (STA). Comput. Geosci. 21 (9), 1091–1104.

Kresic, N., 1995. Remote sensing of tectonic fabric controlling groundwater flow in Dinaric karst. Remote Sens. Environ. 53 (2), 85–90.

Lahti, I., Nykänen, V., Niiranen, T., 2014. Gravity worms in the exploration of epigenetic gold deposits: new insights into the propectivity of the Central Lapland Greenstone Belt, Northern Finland. In: Niiranen, T., Lahti, I., Nykänen, V., Karinen, T. (Eds.), Central Lapland Greenstone Belt 3D Modelling Project Final Report. Geological Survey of Finland, pp. 8–17 Ch. Chapter 1.

Lang, S., 2008. Object-based image analysis for remote sensing application: modeling reality - dealing with complexity. In: Blaschke, T., Lang, S., Hay, G.J. (Eds.), Object-based Image Analysis: Spatial Concepts for Knowledge-driven Remote Sensing Applications. Springer-Verlag, Berlin, pp. 3–27.

Lee, M., Morris, W., Harris, J., Leblanc, G., 2012. An automatic network-extraction algorithm applied to magnetic survey data for the identification and extraction of geologic lineaments. Lead. Edge 26–31.

Leveridge, B.E., Hartley, A.J., 2006. The Varisan Orogeny: the development and deformation of Devonian/Carboniferous basins in SW England and south Wales. In: Brenchley, P.J., Rawson, P.F. (Eds.), The Geology of England and Wales, second ed. The Geological Society, London, pp. 225–256 Ch. 10.

Leveridge, B.E., Holder, M.T., Goode, A.J.J., Scrivener, R.C., Jones, N.S., Merriman, R.J., 2002. Geology of the Plymouth and South-east Cornwall Area, vol. 348 Memoir of the British Geological Survey, Sheet, England and Wales.

Mallast, U., Gloaguen, R., Geyer, S., Rödiger, T., Siebert, C., 2011. Derivation of groundwater flow-paths based on semi-automatic extraction of lineaments from remote sensing data. Hydrol. Earth Syst. Sci. 15 (8), 2665–2678.

Marpu, P.R., Niemeyer, I., Nussbaum, S., Gloaguen, R., 2008. A procedure for automatic object-based classification. In: Blaschke, T., Lang, S., Hay, G.J. (Eds.), Object-based Image Analysis: Spatial Concepts for Knowledge-driven Remote Sensing Applications, pp. 169–184.

Masoud, A., Koike, K., 2006. Tectonic architecture through Landsat-7 ETM+/SRTM DEM-derived lineaments and relationship to the hydrogeologic setting in Siwa region, NW Egypt. J. Afr. Earth Sci. 45 (4–5), 467–477.

Masoud, A., Koike, K., 2017. Applicability of computer-aided comprehensive tool (LINDA: LINeament Detection and Analysis) and shaded digital elevation model for characterizing and interpreting morphotectonic features from lineaments. Comput. Geosci. 106, 89–100.

Mavrantza, O.D., Argialas, D.P., 2008. Object-oriented image analysis for the identification of geologic lineaments. In: In: Blaschke, T., Lang, S., Hay, G.J. (Eds.), Object-based Image Analysis: Spatial Concepts for Knowledge-driven Remote Sensing Applications, vol. 36. Springer-Verlag, Berlin, pp. 383–398.

Middleton, M., Schnur, T., Sorjonen-Ward, P., Hyvönen, E., 2015. Geological lineament interpretation using the Object-Based Image Analysis approach: results of semi-automated analyses versus visual interpretation. Geol. Surv. Finland, Special Paper 57, 135–154.

Miller, H.G., Singh, V., 1994. Potential field tilt-a new concept for location of potential field sources. J. Appl. Geophys. 32 (2–3), 213–217.

Milligan, P.R., Gunn, P.J., 1997. Enhancement and presentation of airborne geophysical data. AGSO J. Aust. Geol. Geophys. 17 (2), 63–75.

Moore, J.M., Camm, S., 1982. Interactive enhancement of Landsat Imagery for structural mapping in tin-tungsten prospecting: a case history of the S.W. England Orefield (U.K.). In: International Symposium on Remote Sensing of Environment, Second

Thematic Conference, Remote Sensing for Exploration Geology. Fort Worth, Texas, December 6 - 10, 1982, pp. 727–740.

Ni, C., Zhang, S., Liu, C., Yan, Y., Li, Y., 2016. Lineament length and density analyses based on the segment tracing algorithm: a case study of the gaosong field in gejiu tin mine, China. Math. Probl Eng. 2016, 1–7. https://www.hindawi.com/journals/mpe/2016/5392453/.

Nixon, C.W., Sanderson, D.J., Bull, J.M., may, 2011. Deformation within a strike-slip fault network at Westward Ho!, Devon U.K.: domino vs conjugate faulting. J. Struct. Geol. 33 (5), 833–843.

O'Leary, D., Friedman, J., Pohn, H., 1976. Lineament, linear, lineation: some proposed new standards for old terms. Geol. Soc. Am. Bull. 87 (10), 1463–1469.

Paananen, M., 2013. Completed lineament interpretation of the olkiluoto region. Tech. Rep. October. Geol. Surv. Finland 1–112.

Peña, S.A., Abdelsalam, M.G., 2006. Orbital remote sensing for geological mapping in southern Tunisia: implication for oil and gas exploration. J. Afr. Earth Sci. 44 (2), 203–219.

Roberts, S., Andrews, J.R., Bull, J.M., Sanderson, D.J., 1993. Slow-spreading ridge-axis tectonics: evidence from the Lizard Complex, UK. Earth Planet Sci. Lett. 116 (1–4), 101–112.

Rogers, J.D., 1997. The Interpretation and Characterisation of Lineaments Identified from Landsat TM Imagery of SW England. Ph.D thesis. University of Plymouth.

Rutzinger, M., Maukisch, M., Petrini-Monteferri, F., 2007. Development of algorithms for the extraction of linear patterns (lineaments) from airborne laser scanning data. In: Proceedings of the Conference 'Geomorphology for the Future', Obergurgl, pp. 1–8 2007.

Scheiber, T., Fredin, O., Viola, G., Jarna, A., Gasser, D., Łapińska-Viola, R., 2015. Manual extraction of bedrock lineaments from high-resolution LiDAR data: methodological bias and human perception. J. Geol. Soc. Sweden (GFF) 137 (4), 362–372.

Scrivener, R.C., Darbyshire, D.P.F., Shepherd, T.J., 1994. Timing and significance of crosscourse mineralization in SW England. J. Geol. Soc., London 151 (4), 587–590.

Shail, R.K., Alexander, A.C., 1997. Late Carboniferous to Triassic reactivation of Variscan basement in the western English Channel: evidence from onshore exposures in south Cornwall. J. Geol. Soc., London 154 (1), 163–168.

Shail, R.K., Leveridge, B.E., 2009. The Rhenohercynian passive margin of SW England: development, inversion and extensional reactivation. Compt. Rendus Geosci. 341, 140–155.

Šilhavý, J., Minár, J., Mentlík, P., Sládek, J., 2016. A new artefacts resistant method for automatic lineament extraction using Multi-Hillshade Hierarchic Clustering (MHHC). Comput. Geosci. 92, 9–20.

Smithurst, L.J.M., 1990. Structural remote sensing of south-west England. Proc. Ussher Soc. 7, 236–241.

Sukumar, M., Venkatesan, N., Babu, C.N.K., 2014. A review of various lineament detection techniques for high resolution satellite images. Int. J. Adv. Res. Comput. Sci. Software Eng. 4 (3), 72–78.

Verduzco, B., Fairhead, D., Green, C.M., MacKenzie, C., 2004. New insights into magnetic derivatives for structural mapping. The Meter Read. 116–119.

Wang, J., Howarth, P.J., 1990. Use of the Hough transform in automated lineament detection. IEEE Trans. Geosci. Rem. Sens. 28 (4), 561–567.

White, J.C., Beamish, D., 2011. Magnetic structural information obtained from the HiRES airborne survey of the Isle of Wight. PGA (Proc. Geol. Assoc.) 122 (5), 781–786.